ISSN1027-5495. Functional Materials, 23, No.2 (2016), p. 236-242
doi:http://dx.doi.org/10.15407/fm23.02.236

The effect of microstructure and the related bio-corrosion behavior Mg alloy in SBF artificial body fluid

Hou Jianbao[1,2], Yao Qi[3], Xiao Yanni[3], Wang Kelu[1,2], Liu Junwei[1,2]

[1] State Key Laboratory of Metastable Materials Science and Technology, Yanshan University, Qinhuangdao 066004, China
[2] Key Laboratory for Microstructural Control of Metallic Materials of Jiangxi Province, Nanchang Hangkong University, 330063
[3] Beijing Spacecraft Manufacturing Factory, Beijing, 100190

Received December 4, 2015

The effect of simulated body fluid (SBF) artificial body fluid on microstructure and morphology characteristics of AZ91D alloy was investigated using OM, SEM and XRD. The effect of corrosion on mechanical properties also was researched. The results show that the corrosion weight loss rate initially increased, then clearly decreased, and finally remained steady. Pits began to appear when the sample was placed in a corrosive environment for five days and pitting gradually increased with longer exposure time. The pits, which made the grain boundaries indistinct, first appeared near the grain boundary area and then gradually increased in area. The main mode of corrosion is pitting and the primary corrosion product, $MgOH_2$, could be observed after five days of corrosion.

Keywords: Mg alloy, artificial body fluid; corrosion; microstructure

Влияние симуляции жидкости организма (SBF) жидкости тела на микроструктуру и морфологические характеристики сплава AZ91D было исследовано с помощью оптической микроскопии, сканирующей электронной микроскопии и рентгеновской дифракции. Исследовано влияние коррозии на механические свойства. Результаты показывают, что скорость потери веса при коррозии вначале возрастает, затем явно уменьшается, и, наконец, сохраняется постоянной. Ямки начинали появляться, когда образец помещали в коррозионную среду на пять дней, и питтинг постепенно возрастал со временем экспозиции. Ямки, которые делали неразличимыми границы зерен, вначале имели площадь сравнимую с границей зерна, а затем постепенно увеличивались по площади. Основным видом коррозии является питтинг, первичный продукт коррозии $MgOH_2$ можно было наблюдать после пяти дней коррозии.

Вплив на мікроструктуру і пов'язана з нею біо-корозійна поведінка магнієвого сплаву в SBF штучної рідини організму. *Хоу Жіанбао, Яо Кі, Хиао Янні, Ванг Келу, Лю Жунвеі*

Вплив симуляції рідини організму (SBF) рідини тіла на мікроструктуру і морфологічні характеристики сплаву AZ91D був досліджений за допомогою оптичної мікроскопії, скануючої електронної мікроскопії і рентгенівської дифракції. Досліджено вплив корозії на механічні властивості. Результати показують, що швидкість втрати ваги при корозії спочатку зростає, потім явно зменшується, і, нарешті, зберігається постійною. Ямки починали з'являтися, коли зразок поміщали в корозійне середовище на п'ять днів, і пітинг поступово зростав з часом експозиції. Ямки, які робили невиразними межі зерен, спочатку мали площу порівнянну з межею зерна, а потім поступово збільшувалися за площею. Основним видом корозії є пітинг, і первинний продукт корозії $MgOH_2$ можна було спостерігати після п'яти днів корозії.

1. Introduction

Due to its high mechanical strength, a matching degradation rate, excellent tissue healing rate and favorable biocompatibilities, magnesium (Mg) and its alloys are good candidates for load bearing degradable biomaterials. Additionally, they have low density and low elastic modulus that are close to those of natural bone. Therefore, extensive studies have been conducted to evaluate the bio-corrosion behavior and biocompatibility of Mg alloys[1-5]. In particular, the common commercial high-purity AZ91D alloy, which has a low cost and a salt spray performance that is close to that of cast aluminum parts, has drawn a lot of attention [5-10].

Witte et al [10] reported on the bio-corrosion behavior and periosteal reactions of four kinds of alloy, including: AZ31, AZ91D, WE43 and LAE442 with a primary alloying composition of 4 wt % Al, 4 wt % Li and 2 wt % RE. It was found that biodegradation reaction occurred on all four kinds of alloy that were implanted in the femoral intramedullary site of a guinea pig [10]. Furthermore, the corrosion layers of Mg alloy in direct contact with the surrounding bone tissue were rich in Ca and P. Compared with reference samples of in polylactic acid, the high rate of mineralization of the adhesion zone surrounded the Mg alloy rods and the weight of bone increased. By 3D-reconstruction it is known that after 18 weeks the AZ91D Mg alloy had almost degraded completely. In Kannan et al, [11] it was reported that the addition of Ca to AZ91D alloy could effectively decrease the corrosion rate and improve significantly its resistance to corrosion. Furthermore, Liu et al, [11,12] reported that by adding protein (BSA) to the solution, the open circuit corrosion potential of AZ91D alloy moved in the cathodic direction, the corrosion was inhibited and then the corrosion resistance of the alloy was improved. The stress corrosion cracking of AZ91D alloy in SBF artificial body fluid was explored by Kannan et al, and it was reported that stress corrosion cracking is not a serious problem for the application of this alloy as implants. Therefore, summarizing these findings, it can be concluded that AZ91D alloy should have huge potential use in the biomedical field.

However, as a biomedical material, the application of AZ91D also entails some difficulties, due to issues such as its low electrochemical potential, active chemical properties, low corrosion resistance, etc. [1-8]. These properties could lead to constraints such as high Mg^+ concentrations, much released hydrogen and subcutaneous emphysema, which bring suffering for patients. Moreover, the biodegradable uncontrollability of AZ91D alloy brings difficulties for biomedical applications. For these reasons it is necessary to explore in detail the bacterial corrosion mechanism and understand precisely the development of the bacterial corrosion process of AZ91D alloy. In particular, in order to comprehend the stress-corrosion performance of AZ91D alloy in the bacterial corrosion environment, it is essential to investigate the evolution of mechanical properties before and after corrosion.

In this study, the effect of simulated body fluid (SBF) on the microstructure and physical characteristics of AZ91D alloy were investigated using a series of test facilities such as optical microscopy (OM), scanning electron microscopy (SEM) and X ray diffraction (XRD). The mechanical properties of the alloy were investigated before and after exposure in the corrosion environment. The related corrosion mechanism of Alloy AZ91D in SBF was explored on the basis of the findings of these tests.

2. Experimental

2.1 Test material

The alloy components were melted under an argon blanket in a mild steel crucible at a temperature of 690°C with a holding time of 30 min. Following the melting and alloying processes, the molten AZ91D alloy, whose composition is shown in Table 1, was poured into a pre-heated steel mould to produce ingots of the alloy. The melted AZ91D rod (purity better than 99.9%) was cut into 10mm×10mm×5mm pieces after a homogenization treatment. Subsequently, the samples were cleaned ultrasonically in acetone for ten minutes to remove grease.

2.2 SBF preparation

The components of the SBF solution were as follows: 8.035g/L NaCl + 0.335g/L $NaHCO_3$ + 0.225g/L KCl + 0.231g/L K2HPO4·3H2O + 0.311g/L $MgCl_2 \cdot 6H_2O$ + 39ml HCl 1mol/L+ 0.292g/L $CaCl_2$ + 0.072g/L Na_2SO_4 + 6.118g/L Tris + 0-5ml HCl (1mol/L).

2.3 expermental procedure

The alloy samples were immersed in the SBF solution and parameters such as pH and

Table 1. Chemical composition (wt%) of AZ91D magnesium alloy

Al	Zn	Mn	Si	Cu	Ni	Fe	Be
9.0889	0.6411	0.2043	0.0393	0.0010	0.0007	0.0022	0.0006

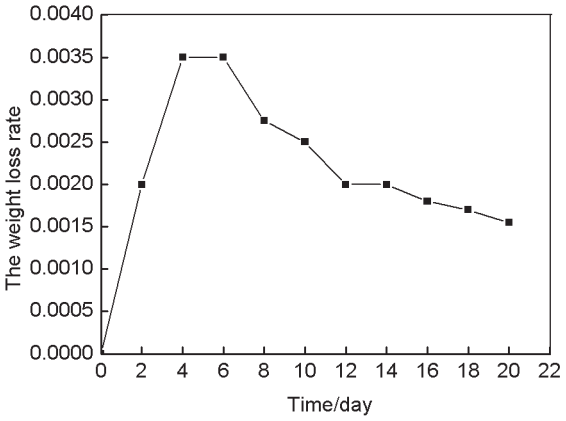

Fig. 1 Corrosion weight loss rate curve of AZ91D alloy

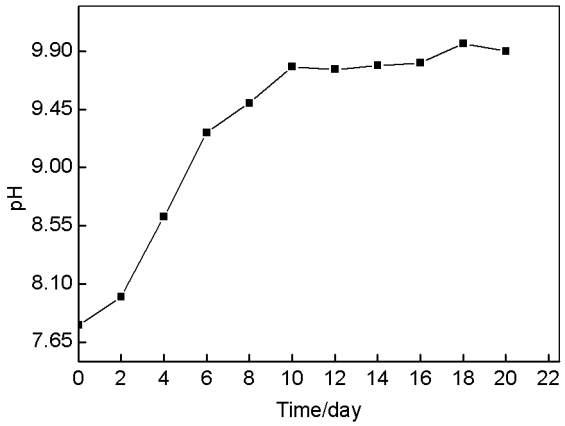

Fig. 2. Change in pH for AZ91D alloy immersed in SBF

weight loss were measured every day. Before weighing, the samples were taken out of the BSF solution and washed using chromic acid solution (200g/L CrO_3+10g/L $AgNO_3$), cleaned in an ultrasound bath and washed with distilled water and dried. An electronic balance (BT-224S) was used to weigh the dry samples.

Other bulk and tensile samples were immersed in the SBF solution and the solution was replaced every day. Different samples were taken out from SBF solution every day and washed in chromic acid solution (200g/L CrO_3 + 10g/L $AgNO_3$), cleaned ultrasonically in distilled water and dried. The microstructure of the samples was investigated using OM (XJP-6A) and SEM (Quanta200) and the appearance was recorded using a camera. XRD was used to explore the characteristics of the corrosion product. The content of the metallographic etchant solution was: 4.2g chrysolepic acid + 70ml absolute ethyl alcohol + 10ml glacial acetic acid + 10ml distilled water. In order to evaluate the stress-corrosion performance of AZ91D alloy in the bacterial corrosion environment, the evolution of mechanical properties before and after corrosion was investigated.

3. Results

3.1 pH values and weight loss rates

Table 2 shows the weight change of AZ91D alloy with corrosion time.

It can be observed that due to the change in the conductivity of the solution, the weight continuously decreases with time. The corrosion rates can be calculated using the weight loss method whose formula is shown as follows, and a plot of the weight loss results can be seen in Figure 1[6]:

$$v = \frac{m_0 - m_1}{A \cdot T} \quad (1)$$

Table 2. Sample mass change of AZ91D alloy

Time/ day	0	2	4	6	8	10
Mass/g	3.034	3.03	3.02	3.013	3.012	3.009
Time/ day	12	14	16	18	20	
Mass/g	3.009	3.005	3.005	3.003	3.003	

where m_0 is the sample weight before corrosion; m_1 is the sample weight after removal of the corrosion product; A is the surface area of the sample; T is the immersion time and v is weight loss rate in g/cm^2 day.

It can be observed from Figure 1 that the weight loss rate of AZ91D alloy increased rapidly with until the fifth day and then decreased significantly until the eleventh day. Thereafter, the curve tended to remain steady and there is little further change during the last days of the test. The corresponding trend plot of the pH values is shown in Figure 2 and it is known from this that the pH increases rapidly during the first period until the fifth day and then the tendency for increase slows during the second stage until the eleventh day.

3.2 Macro morphology

The samples were immersed in SBF solution and one of them was taken out every other day whose macro morphology was shown in Fig 3. It can be seen from Fig3 that the surface of the samples gradually become deep with time and the degree of corrosion also become serious before the first eleven days. Nevertheless, the surface of samples has no obvious change after 12 days and the results are in accordance with Fig. 1 and Fig. 2. By the macro morphology of the second, the fourth and the eighth days, it can be seen that the corrosion occurs from boundary of the sample and gradually extend gradually to internal. This is because that the

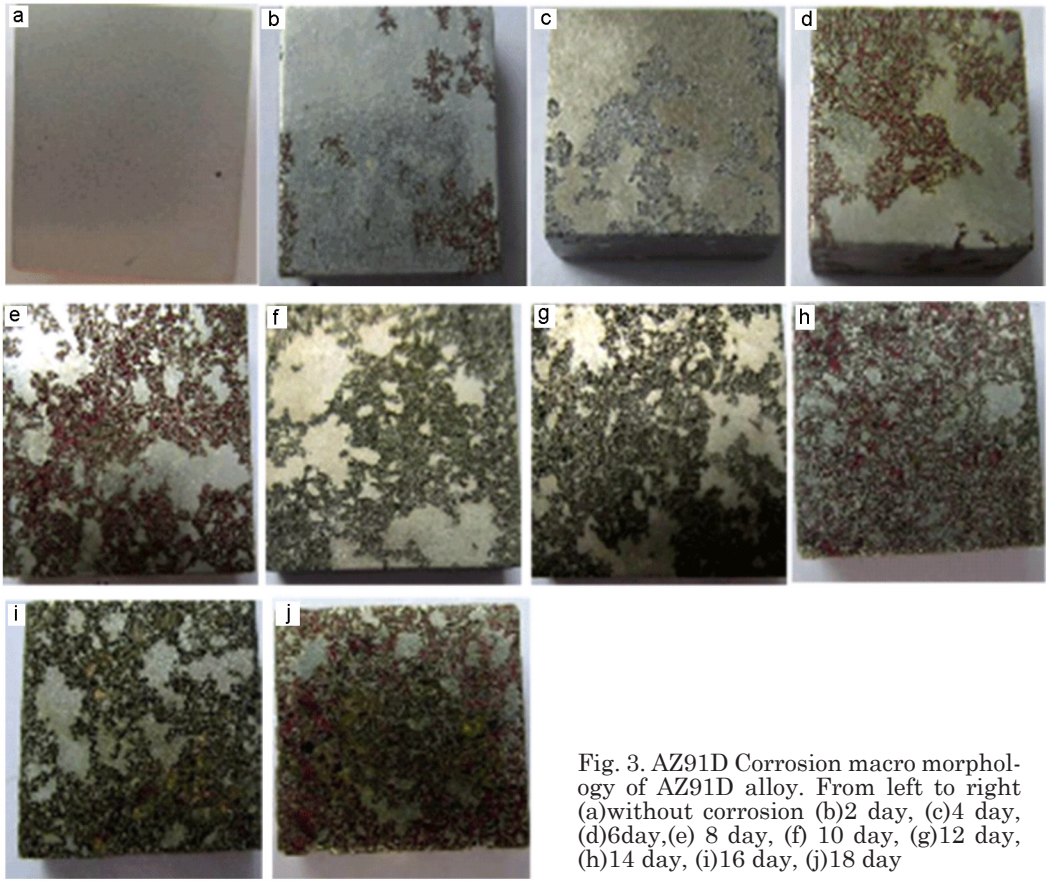

Fig. 3. AZ91D Corrosion macro morphology of AZ91D alloy. From left to right (a)without corrosion (b)2 day, (c)4 day, (d)6day,(e) 8 day, (f) 10 day, (g)12 day, (h)14 day, (i)16 day, (j)18 day

polish level of four side faces is lower than the investigated face and the four side faces can easily be corroded firstly.

3.2 Microstructure

The microstructure of the sample before immersion and after exposure for 4 days, 10 days and 20 days is shown in Figures 3.

It can be observed that the grain boundaries have become thick and pits have begun to appear near the grain boundaries. As is evident from Figure 4(b), pits become very evident during the first four days. The pits that make the grain boundaries indistinct first appear near the grain boundary area and then expand gradually, as shown in Figure 4(c). As compared to the sample that was corroded for four days, shown in Figure 4(b), the amount of pits on the samples corroded for eleven and twenty days increased significantly, as shown in Figures 4(c) and 4(d). In Figures 4(c) and 4(d), most of micropits connect with each other and then nearly fill the entire field of view.

3.3. SEM imgine

Figures 4 show SEM images of samples before and after immersion.

In Figure 5(a), almost no corrosion is evident and the width of grain boundary is narrow. After the twenty-day immersion period corrosion, a thick corrosion layer can be observed and cracking is evident, as is shown in Figures 5(b) and 5(c). The most prevalent type of attack is pitting.

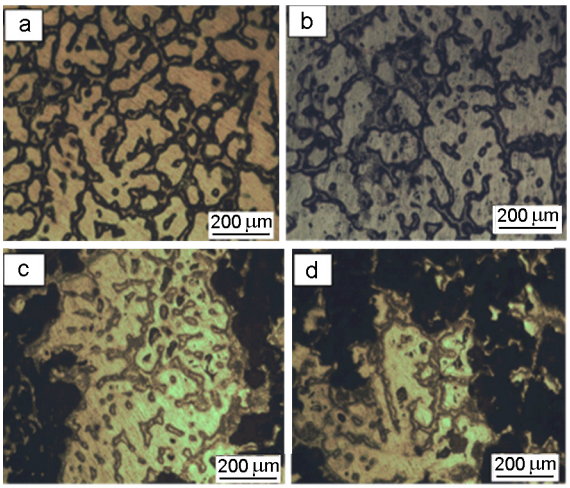

Fig. 4. Microstructure of AZ91D alloy before and after corrosion. (a)Without corrosion (b) After 4 days (c) After 10 days (d) After 20 days

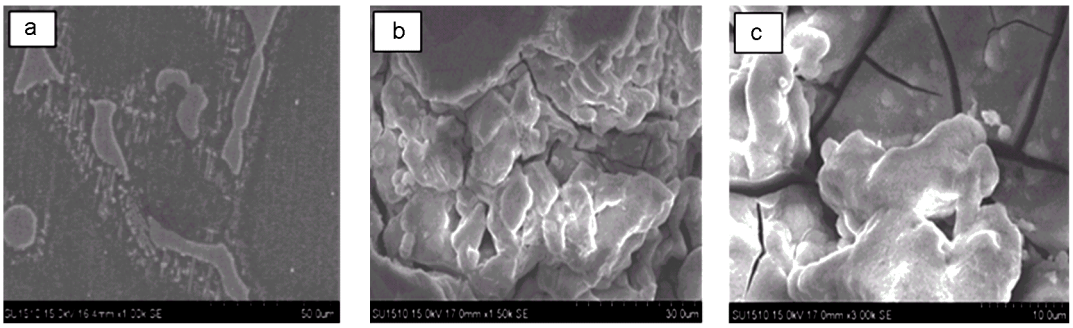

Fig. 5. SEM images of corrosion specimens. (a) Without corrosion, (b) and (c) After 20 days

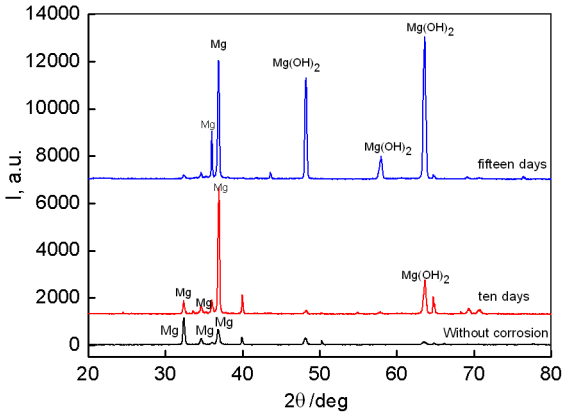

Fig. 6. XRD traces for specimens before and after immersion in SBF

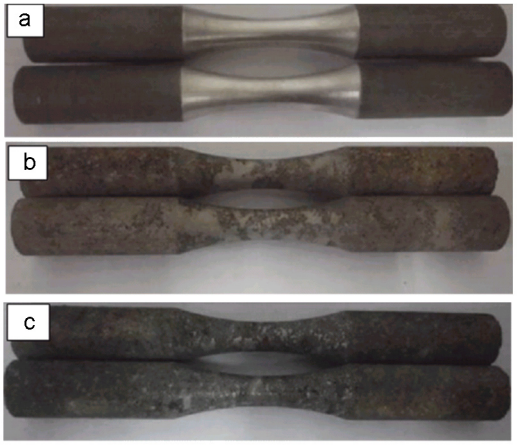

Fig. 7. Macroscopic samples after corrosion of AZ91D alloy. (a) Without corrosion, (b) 4 days, (c) 8d ays

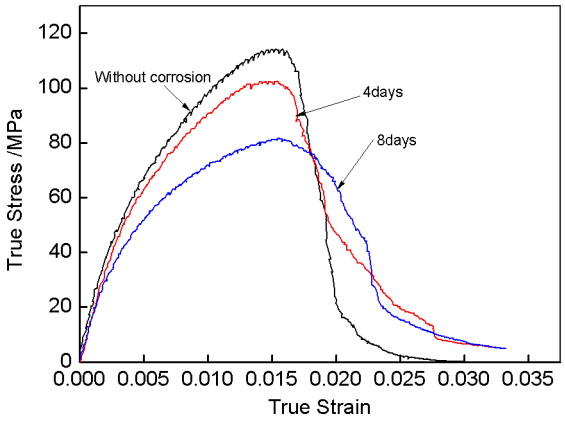

Fig. 8. True stress- strain curve of AZ91D alloy with strain rate $10^{-2}s^{-1}$

3.4 XRD analysis

The XRD patterns of the samples before and after corrosion are shown in Figure 6.

It is evident that no corrosion product can be observed for the original sample and three strongest peaks are from the α-Mg matrix. When the sample was corroded for ten days, the peak of the new phase $MgOH_2$ is present, which means the proportion of $MgOH_2$ had increased. After corrosion for fifteen days, the $MgOH_2$ peaks are still higher. Of the three strongest peaks in XRD trace, two peaks belong to $MgOH_2$.

3.5 Mechanical properties

The macro morphology of tensile samples before and after corrosion with 4 and 8 days was shown in Fig. 7. It is known from Fig. 7 that the degree of corrosion gradually becomes serious and the etch pits increase with corrosion time expanding. The stress-strain curve with strain rate 10^{-2} s^{-1} and peak stress values of these samples was shown in Fig. 8 and Table 2.

Table 3. Peak stress values of AZ91D alloy (MPa)

original sample	4days	8days
111	99	80

It can be observed form Fig. 8 and Tabe 3 that the values of peak stress decrease with corrosion time expanding. It can be mainly credited to the increase of etch pits which can induce the emergence of crack source.

3.6 Frature morphology

The fracture morphology of the tensile samples before and after corrosion was shown in Fig. 9. It can be seen that the fracture mechanisms of these samples gradually changed. In

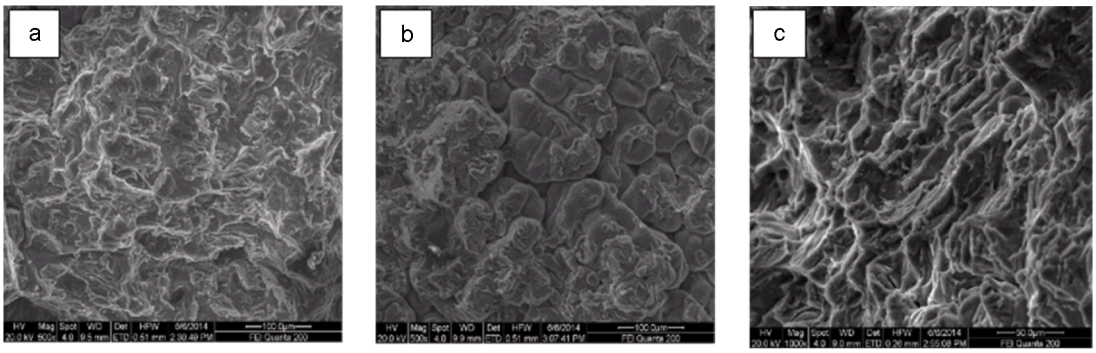

Fig. 9. The fracture morphology of the tensile samples before and after corrosion

Fig. 9 (a), the main fracture way is mainly dimple fracture which belong to plastic fracture and lots of dimples can be observed. However, the fracture way gradually changed for the tensile sample corroded with 4 days and the main fracture way is mixture of quasicleavage and touph dimple, as shown in Fig. 9 (b). In Fig. 9 (c), the main fracture way has changed to cleavage fracture and lots of cleavage facets can be observed. The evolution of fracture mechanism can also be credited to the occurrence of etch pits which can induce the emergence of crack source.

4. Discussion

During the last days of the test, the pH value basically remained steady. Therefore, based on the above, it can be concluded that the tendency for the increase in pH mirrors the change in corrosion rate. The reason for this phenomenon is the significant effect of pH on the corrosion of the Mg alloy[9-12].

The effect of pH can be divided into two ranges. When the corrosion occurred during the first few days, the pH value was lower than 10.5 and the main reactions were hydrogen evolution and the dissolution of the Mg [12]. Then, due to the production of OH- during the dissolution, the pH value of the solution increased significantly. When a pH value between 10.5 and 12 was attained, the corrosion potential and current were relatively stable, that resulted in a slowing of the corrosion reaction.

Aluminum is the most important solution element in Mg-Al alloys and the biggest solubility of Al in pure Mg is 12.7% when the temperature is 437K. While when the temperature decreases to room temperature, the solubility of Al is only about 2%[13]. Hence, the microstructure of the AZ91D alloy at room temperature mainly includes α solid solution and the γ-$Mg_{17}Al_{12}$ precipitated phase. Nevertheless, in the actual solidification conditions, due to the high content of Al in AZ91D alloy, a little eutectic structure also appears at the boundary of α-Mg grains.

Owing to the difference in corrosion potential for these phases (pure Mg 1.55V and γ-$Mg_{17}Al_{12}$ precipitated phase 1.31V), a virtual battery is formed between α-Mg matrix and the γ-$Mg_{17}Al_{12}$ precipitate phase when the alloy is immersed in a corrosive environment [13]. In the couple, α-Mg matrix is the anode and the γ-$Mg_{17}Al_{12}$ precipitated phase is the cathode. Therefore, three results could be concluded:

– γ-$Mg_{17}Al_{12}$ precipitated phase is helpful for the generation of micro pits.

– Compared to the γ-$Mg_{17}Al_{12}$ precipitated phase, the α-Mg matrix is easily corroded and the chemical equation is $Mg = Mg^{2+} + 2e^{-}$.

– The initial micro pits appear in the area of α-Mg matrix area near grain boundaries [14-15].

Hence, at the beginning of the corrosion process, along with the dissolution of Mg matrix, fine micro pits appear near grain boundaries, which appear to broaden and thicken. Then, coarse black pits gradually appear.

An oxide film can be formed in natural state on the reactive Mg alloy that hinders subsequent attack. However, Cl^- ions can seriously damage the stability of the oxide film and if the concentration of Cl^- ions is between 2mol/L and 200 mol/L, pitting corrosion will occur [14]. The concentration of Cl^- ions in SBF is 140mol/L and this leads to two kinds of damage. The γ-$Mg_{17}Al_{12}$ on the Mg alloy will attach to the surface of matrix, but can not cover the whole matrix surface. Therefore, the cracking is produced in these corrosion product deposits, as shown in Figures 4(b) and 4(c).

5. Conclusion

In this investigation, the effect of SBF artificial body fluid on the microstructure and morphology of AZ91D alloy were investigated. The associated corrosion mechanism in SBF was evaluated and the effect of corrosion on the mechanical properties of the alloy was explored.

The conclusions of the study are summarized as follows:

– During immersion in SBF, the rate of weight loss initially increases, then decreases until the eleventh day, and thereafter remains steady. During this period, the pH value of the solution initially increases until the eleventh day and thereafter remains steady.

– Micro pits began to appear when the sample had been immersed for five days and gradually increased with longer immersion time. The micro pits that make grain boundaries indistinct firstly appear near the grain boundary area and then gradually increase in size.

– The primary morphology of corrosion is pitting attack and main etching product is $Mg(OH)_2$ which can be observed after five days of immersion.

Acknowlesgementes

The investigation was supported by National natural science Foundation of China(Grant No.51504138); the Open Project of State Key Laboratory of Metastable Materials Science and Technology (201405); the Science and Technology Support Program of Jiangxi Province (20141122040007); the Shanghai Aerospace Science and Technology Foundation (SAST201328); the Aerospace Science and Technology Foundation (BA201401259);the Key Laboratory for Microstructural Control of Metallic Materials of Jiangxi Province (Nanchang Hang Kong University) (LW201101). the Youth Science Foundation of Jiangxi Province (20141522040222) and the Natural Science Foundation of Jiangxi Province(20122B AB216015).

References

1. **T. Zhou, D. Chen, Z-H. Chen,** *Transactions of Nonferrous Metals Society of China,* **18**, 101, 2008.
2. **J-W. Liu, D. Chen,** *Transactions of Nonferrous Metals Society of China,* (S1), 2008.
3. **Z-H. Yu, H-G. Yan, X-Y. Yin,** *Transactions of Nonferrous Metals Society of China*, **22**, 2012.
4. **J. Zhang, D-W. Zhou,** *Transactions of Nonferrous Metals Society of China,* **19**,205, 2009.
5. **D-W. Zhou, J-S. Liu, J. Zhang,** *Transactions of Nonferrous Metals Society of China*, **2**,250, 2007.
6. **S. I. Rokhlin, J.-Y. Kim, H. Nagy, B. Zoofan,** *Eng. Fracture Mech.,* **62**, 425,1999.
7. **A. Eliezer, E. M. Gutman, E. Abramov,** Y. Unigovski, *J.Light Metal.*, **1**, 179, 2001.
8. **Y. Unigovski, A. Eliezer, E. Abramov, Y. Snir, E.** M. Gutman, *Mater.Eng.* **A**, **360**,132, 2003.
9. **M. S Bhuiyan, Y. Mutoh, T. Murai,** *Intern. J. Fatigue,* **30**, 1765, 2008.
10. **F. Witte, V. Kaese, H. Haferkamp,** *Biomaterials,* **26**, 3557, 2005.
11. **M. B. Kannan, R. K. S Raman,** *Biomaterials,* **29**, 2306, 2008.
12. **C-L. Liu, Y-C. Xin, G-Y. Tang, P-K. Chu,** *Mater. Scie. Engin.* **A , 456,** 350, 2007.
13. **M. B. Kannan, R. K. S. Raman,** *Scripta Mater,* **59**, 175, 2008.
14. **M. P. Staigera, A. M. Pietaka,** *Biomaterials*, **27**, 2006.
15. **P. Muthukumar, Maiya, M. Prakash, S. Srini**rasa Murthy, **R. Vijay, R. Sundaresan,** *J. Alloys Comp.,* **452**, 456, 2008.